**East African Scholars Journal of Agriculture and Life Sciences**
*Abbreviated Key Title: East African Scholars J Agri Life Sci*
ISSN 2617-4472 (Print) | ISSN 2617-7277 (Online)
Published By East African Scholars Publisher, Kenya

Volume-3 | Issue-6 | June-2020 | DOI:10.36349/EASJALS.2020.v03i06.008

OPEN ACCESS

**Research Article**

# Using Spectral Indices for Drawing Fire Occurrence (Wheat crop) in Diyala (Eastern Iraq) Using Landsat-8 imagery Airborne Simulator Data

Modher H. Abd*[1] and Saif J. Kadhim[2]

[1]Agriculture Directorate of Najaf, Iraq
[2]Ministers of Construction & Housing, Baghdad, Iraq

**Article History**
**Received:** 05.06.2020
**Accepted:** 11.06.2020
**Published**: 26.06.2020

**Journal homepage:**
http://www.easpublisher.com/easjals/

**Quick Response Code**

**Abstract:** This paper tried to detect a burned area that occurred in the Diyala region of Eastern Iraq. In the past, forest and land fire not mostly occur in Iraq. During this time, it is possible that this phenomenon also occurs due to the existence of terrorism, especially the destruction of agriculture regions of the Wheat crop. The data used were Landsat-8, the latest generation of the Landsat series. The research methods include Mosaic method, Clip method, Atmospheric Correction, reflectance pattern analysis, Normalized Difference Vegetation Index (NDVI) and Normalized Burn Ratio (NBR) extraction, separability analysis. The results show that P1, P2, P5 , NBRs and NBRL parameter shows the highest values of D-values (most sensitive), to detect the burned area. Then, compared to P1, P2, P5, and NBRs, Normalized Burn Ratio long (NBRL) provide better results in detecting burned areas.

**Keywords:** Burned area, Fires, NDVI, NBR, Remote sensing



## INTRODUCTION

Every year (2.5-4.0 million km2) of vegetation is burned around the world, where emitting an annual average of 2,013 Tg of Carbon. Incidents of burning wheat and barley fields in the provinces of Diyala, Salah al-Din and Ninewa caused significant material losses. According to a report by the Ministry of Planning in 2019, the area planted with wheat crop was 3154 dunums, and the average cultivated area of the crop (690.5 kg per dunum). In Iraq, the official statistics of burned areas are not well known, but fires facing farmers have fluctuated this year; the country needs to reach a self-sufficiency phase of wheat, 4.2 million tons a year.

The latest generation satellite of the Landsat series Landsat-8. it has been widely used to identified and mapped forest and land fires. But, most research took place in forest regions, such as Sumatera, southern African, Southern California and of Kalimantan in Indonesia regions. This research aimed to detect the burned area that occurred in the Diyala (Eastern Iraq) region using Landsat-8. This report raises the subject of how remote sensing image data can be used in the product information on the distribution and extent of burned areas. This burned area knowledge is significant information for estimating impact and damage assessments, and for preparing the policy or mitigation programs to prevent Wheat cropland fires.

## LITERATURE REVIEW

The work of (Suwarsono, H. L. *et al.*, 2018), showed to detect a burned area that occurred in (Northeast slope of Mt. Ijen Java Island). done used Landsat-8 data, where the method included radiometric correction(R c), data fusion(Df), sample training retrieval(STR), reflectance pattern analysis(RPA), Normalized Difference Vegetation Index (NDVI) and Normalized Burn Ratio (NBR) extraction, separability analysis(SA), and parameter selection for burned area detection by ArcGIS. The results display that (NBRL) and (ρ5) parameter shows the highest values of (D) values. Then, Normalized Burn Ratio long (NBRL) provide better results in detecting burned areas.

The report of (Anaya, J. A. *et al.*, 2018), estimates temporal methods to improve burned area detection utilize Landsat 5-TM and landsat8-OLI, where the normalized burn ratio (NBR) was used. For maximizing the burned area detection two alternatives

***Corresponding Author:** Modher H. Abd

were evaluated: use of time-series metrics and the relative form of the temporal difference (RdNBR). Three areas of Latin America with large fire were selected: Colombia (Amazon Forest), Bolivia (the transition from Chiquitano to Amazon Forest), and Argentina(El Chaco Region). The accuracy estimate of these new products was based on burned area protocols. Finally. The best model classified 85% of burned areas in Bolivia, 69% of burned areas in Argentina and 63% of the burned areas of Colombia.

The research of (Long, T. *et al.,* 2019), focuses on an automated global burned area mapping (BAM) approach depend on Landsat images(the huge catalog during 2014–2015 ) and various spectral indices were used (NDVI filter, Normalized Burned Ratio (NBR) filter, and temporal filter) to calculate the burned probability of each pixel using random decision forests by Google Earth Engine. Finally, product found a similar spatial distribution and a strong correlation ( R 2 = 0.74) between the burned areas from the two products, although differences were found in particular in agriculture land.

The study of (González-Alonso, F. *et al.,* 2013), the development and application of a new algorithm for mapping burned areas in Colombia, using a synergistic combination of reflectance images ( MODIS sensors installed on NASA 's TERRA and AQUA ). after , apply and validation found a burned surface area in Orinoquía of 998,473 (ha) was obtained for the month of February 2007and the algorithm was performed using high spatial resolution Landsat images. then, the comparison of the data with the global MODIS MCD45A1 burned area product. The results, the algorithm performed very similar to MCD45A1, with an overall accuracy of 79% in both cases.

In this paper (Todd, J. *et al.,* 2017), we present an algorithm that identifies burned areas in dense time-series of Landsat data to produce the Landsat Burned area, where the algorithm uses gradient boosted regression models using band values and spectral indices from individual Landsat scenes. BAECV products were generated for the conterminous United States from (1984 - 2015) with pixel-level burn probabilities for each Landsat scene. done compared the BAECV burn classification products GFED (1997–2015) and MTBS (1984–2013) data. The results found that the BAECV 36% more burned area than the GFED and 116% more burned area than MTBS. in addition, differences between the BAECV products and the GFED (32% and 88% more burned area), respectively. Finally, there was anticipate the BAECV products will be useful to studies that seek to understand past patterns of fire occurrence.

The article of (Nugroho, J. T., & Arifin, S. 2014, September), aims to obtain the best model parameters for burned areas(BA) using Landsat-8. Finally, the results show NBR gave the best results compared to other parameters.

The work of (Trisakti, B. *et al.,* 2017), to develop a method for burned area mapping that happened between two Landsat-8 data recording on August 13th and September 14th, 2015. Samples were taken at several land covers to determine the spectral pattern differences .then, the analysis was performed to determine the suitable spectral bands or indices and threshold values. The results showed that soil was extracted using ratio SWIR / NIR , and the burned area was extracted using a combination of NIR and SWIR band.

The report of (Roy, D. P. *et al.,* 2019), presents a combined Landsat-8 Sentinel-2 burned area mapping algorithm, where The different sensor data are combined through a random forest change regression. Then, the random forest regression is applied independently at each gridded 30 m pixel location on a temporally rolling basis.in addition, The results are compared with contemporaneous NASA MODIS fire products to gain insights into their temporal and spatial reporting differences. the finally, The results mapped less area burned than the interpreted maps, as reflected by a (0.24) omission error and a negative relative bias (−0.19), with a small (0.06) commission error.

In this paper (Vedovato, L. B. *et al.,* 2015), compare two different methodologies(the Normalized Burn Ratio (NBR) and the Linear Spectral Mixture Model (SMM)data extracted from Landsat -8 image ) of fire detection for the Amazon region .then, evaluate possible spectral confusions these two methods. The results refer that the detection of burned forest areas with the LSMM index performs better over fragmented landscapes(Kappa of 0.68 and 0.66) against an index NBR (Kappa of 0.52 and 0.52). Finally, the LSMM index is likely to perform better in the detection of burnt forests than the NBR index.

**Study Area:**

The spatial location of Diyala province is the central region of Iraq to the east of the Tigris River, it runs between two circles(33-36N and 44-48E) as shown (Fig. 1.). The study area is characterized hot dry summers and cold winters, where the characteristics of the continental climate are clear the region's rains have little to do with, and fewer rains make them more like the semi-desert climate system. The region is characterized by diversity in the terrain, where there are mountains, floods and plateaus and this difference created a distinction for the regions of the province and different from each other in the elements of climate, and was the cause of direct and indirect impact on the development of water resources and the establishment of irrigation projects. The impact on the life of the citizen where Diyala province decades before the richest provinces of the country because of the availability of water and the development of irrigation

projects. Surface and terrain shapes play an influential role in services helps the process of leveling, plowing, harvesting, and extending water systems. The mountainous area is separated from the plain by the Hamrin Mountain Range, which extends 150 km inside the governorate. The Hamrain Range is the longest chain in Iraq and these hills are poor with vegetation, grass and livestock because of the very small amounts of rain.

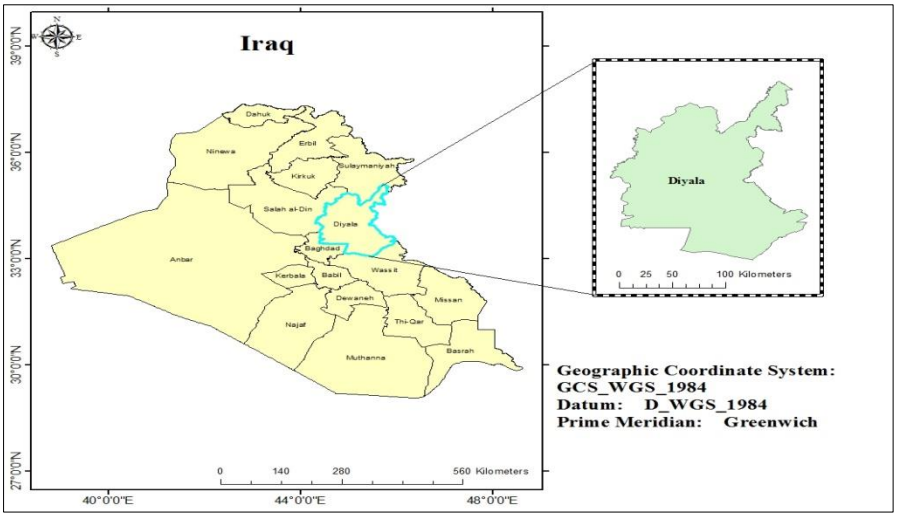


**Fig. 1.** Study area

## METHODOLOGY

The research methods include **Mosaic method**, **Clip method**, **Atmospheric Correction,** reflectance pattern analysis, Normalized Difference Vegetation Index (NDVI) and Normalized Burn Ratio (NBR) extraction, separability analysis, parameter selection for burned area detection, parameter test, and evaluation.

**Mosaic Method:**

A project was created to include(2) images for a cover study area, the datum were chosen WGS-84. The tool mosaic (multiple input raster into an existing raster dataset) was applied to the project, as shown Fig.2 by software ArcGIS10.2.2.

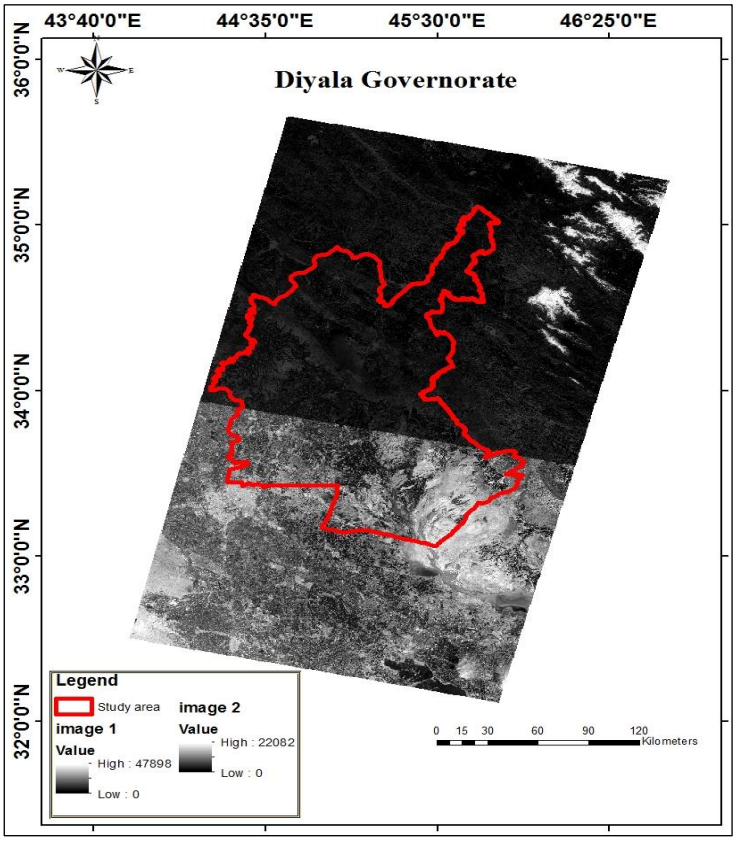


**Fig.2.** Mosaic method

**Clip Method :**

This tool is to cut out a piece (raster data set) of one feature class(shape file study area). This is particularly useful for creating a new feature class—also referred to a study area or area of interest (AOI).

**Atmospheric Correction:**

As the utility of these data, converts more quantitative and accurate recovery of surface reflectance becomes increasingly important. Fortunately, a very small percentage of contaminated aerosols, clouds, and cloud shadows are represented in this study(Our region is free of cloud and land cloud cover 0.07 for scenes). If Landsat-8 images contain a very large percentage of these contaminates can be actually more suitable when aerosols, clouds, and cloud shadows can be removed (Liang, S. *et al.*, 2001).

**Reflectance Pattern Analysis :**

The satellite images are produced as digital numbers. Then, the digital number (DN) is converted to reflections and the result is a clear represented surface reflection according to the Eq. (1 and 2) (Landsat, U. S. G. S. 2015).

$$\rho\lambda' = M^{\rho} * Qcal + A^{\rho} \quad (1)$$

Where:
$\rho\lambda'$ = Top-of-Atmosphere Planetary Spectral Reflectance, without correction for solar angle.
$M^{\rho}$ = Reflectance multiplicative scaling factor for the band (REFLECTANCEW _ MULT_BAND_n from the metadata).
$A^{\rho}$ = Reflectance additive scaling factor for the band (REFLECTANCE _ ADD_BAND_N from the metadata).
Qcal = Level -1 pixel value in DN.

Note:
That $\rho\lambda'$ is not true TOA Reflectance because it does not contain a correction for the solar elevation angle (Zanter,2015). The conversion to true TOA Reflectance formula is:

$$P\lambda = \rho\lambda'/\sin(\theta) \quad (2)$$

Where:
$P\lambda$ = Top-of-Atmosphere Planetary Reflectance.
$\theta$ = Solar Elevation Angle (from the metadata).

The level of preprocessing necessary will rely on the problem to which the processed images are to be applied. Therefore, no fixed schedule of preprocessing operations that are carried out automatically prior to the use of remotely-sensed data.

**Normalized Difference Vegetation Index (NDVI):**

Is an index of plant green or photosynthetic activity

The following equation is used to extract the NDVI (Gao, B. C. 1995):

$$\mathbf{NDVI} = \frac{P5 - P4}{P5 + P4} \quad (3)$$

Where:
**NDVI** is Normalized Difference Vegetation Index.
P4 and P5 are reflectance value of band 4, and 5 respectively.

**Normalized Burn Ratio Short (NBRs):**
The following equation is used to extract the NBRs (Key, C. H., & Benson, N. C. 1999):

$$\mathbf{NBRs} = \frac{P6 - P5}{P6 + P5} \quad (4)$$

Where:
**NBRs** is Normalized Burn Ratio (short).
P5 and P6 are reflectance value of band 5, and 6 respectively.

**Normalized Burn Ratio Long (NBRL):**

The following equation is used to extract the NBRL (Key, C. H., & Benson, N. C. 1999):

$$\mathbf{NBRL} = \frac{P7 - P5}{P7 + P5} \quad (5)$$

Where:
**NBRL** is Normalized Burn Ratio (long) .
P5 and P7 are reflectance value of band 5, and 7 respectively.

**The Separability (D):**

The following equation is used to measure the separability (Rouse, J. W. *et al.*, 1974) :

$$\mathbf{D} = \left| \frac{M2 - M1}{S2 - S1} \right| \quad (6)$$

Where D is the Normalized Distance, M1 and M2 are mean values of samples before and after eruption respectively, S1 and S2 are the deviation standard of samples before and after eruption respectively.

## RESULTS AND DISCUSSION

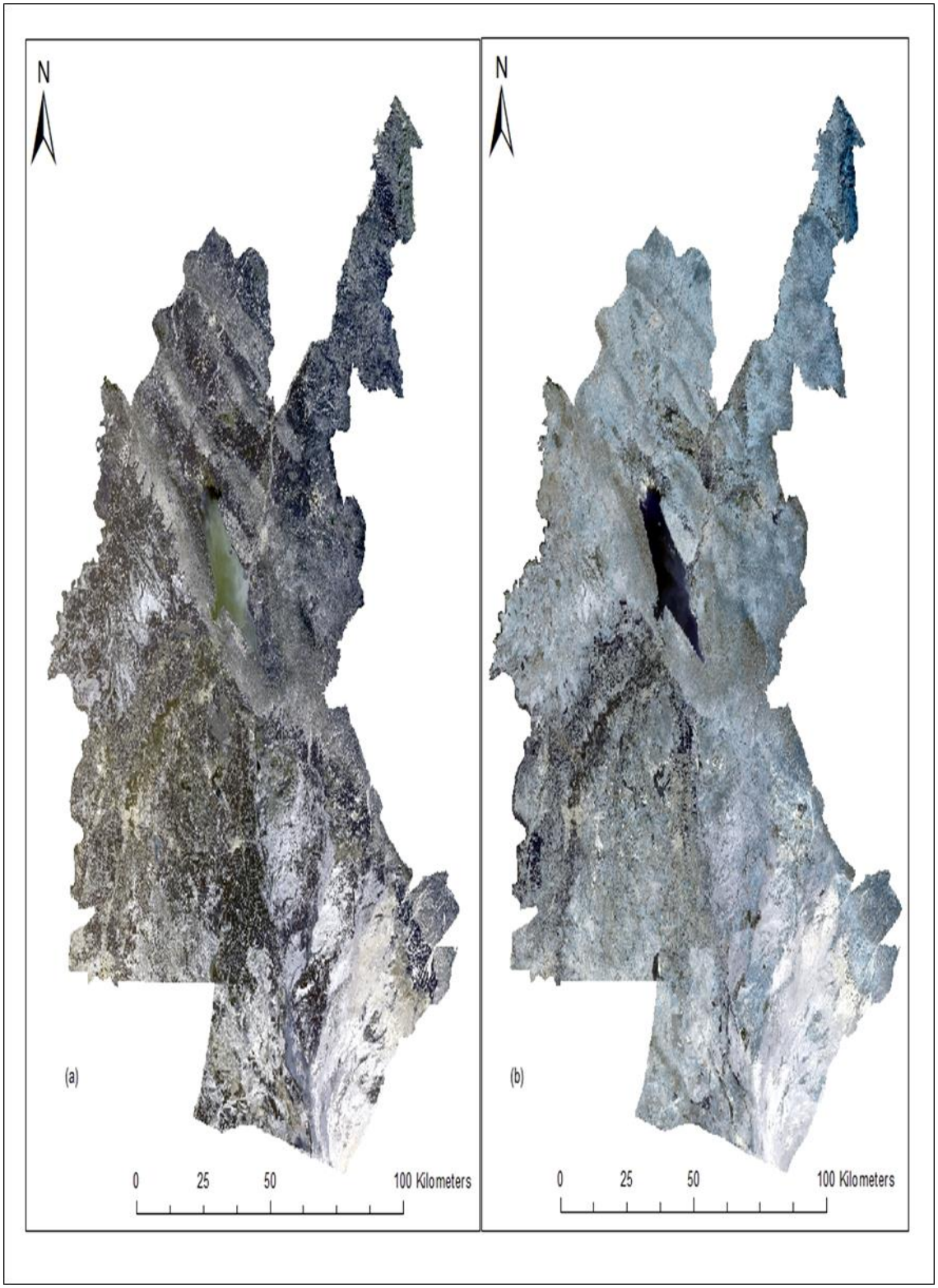


**Fig. 3.** Landsat-8 RGB 654 Diyala date of March 21, 2019 (pre-fires) and September 13, 2019 (post-fires).

A pair of Landsat-8 date March 21, 2019, and September 13, 2019, showed the affected area due to fires in the Diyala Region. From the color composite band RGB 654 Fig .3, there can be identified the burned areas during that period. Burned areas show the black color and look small shape.

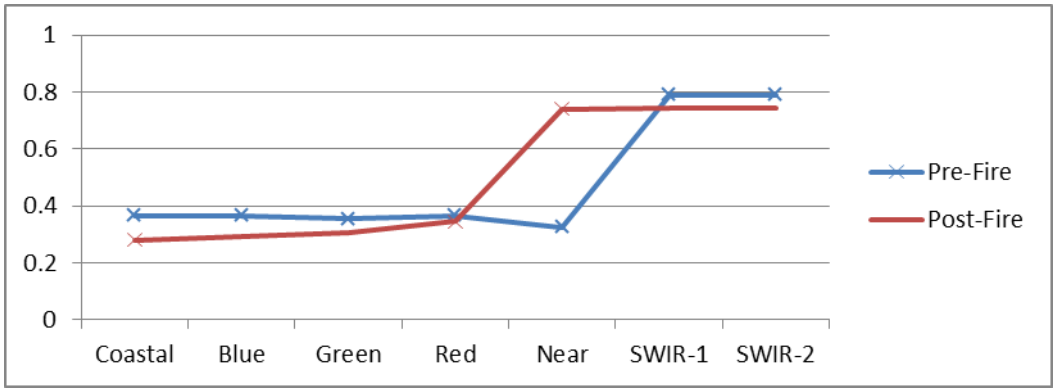


**Fig. 4.** The reflectance values of the burned area due to the fires between March 21, 2019 (pre-fires) and September 13, 2019 (post-fires).

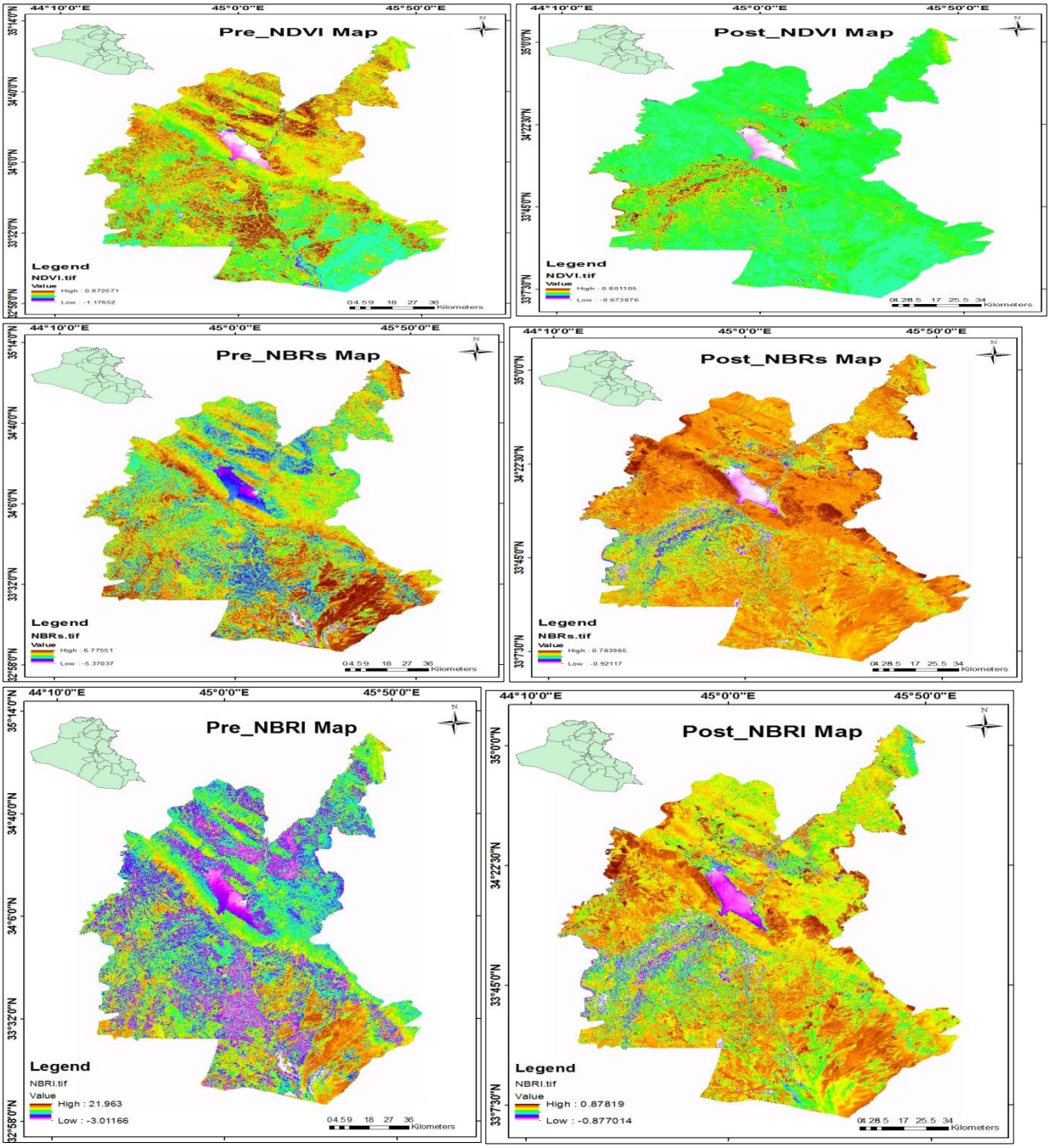

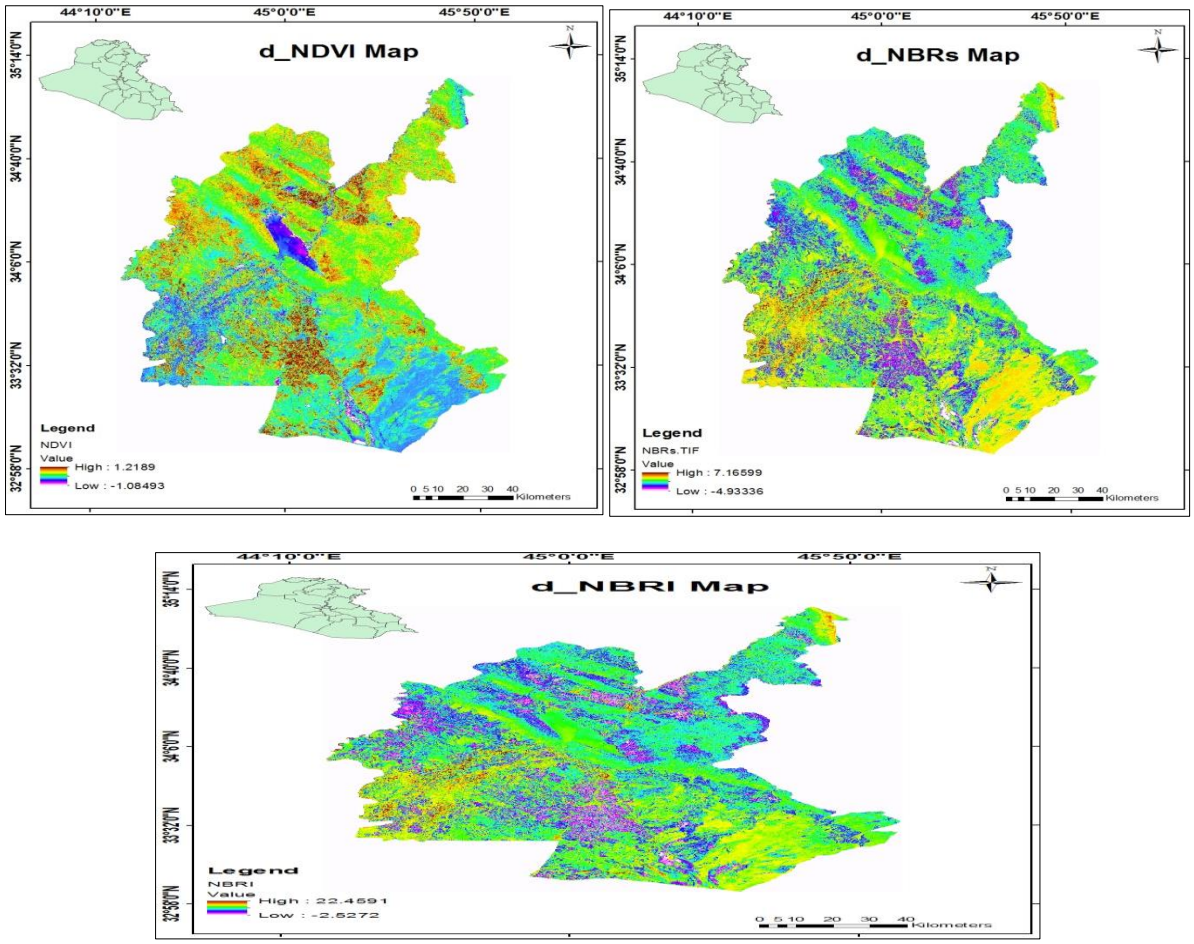


**Fig.5.** Pre-fires and post-fires images of NDVI, NBRS, and NBRI derived from Landsat-8

Several training areas of burned areas took in both derived reflectance corrected images. Then we measured the statistics of reflectance values from Band1, Band2, Band3, Band4, Band5, Band6 and Band7. In addition, measurements were made for NDVI, NBRS and NBRL images. Fig .4 and Table1 showed the Landsat-8 OLI reflectance as well as index values of the burned area due to the fires between March 21, 2019 (pre-fires) and September 13, 2019 (post-fires).

**Table1.** The changes in reflectance and index values due to fires

| **Pre-Fire** | | | | | | | | | | |
|---|---|---|---|---|---|---|---|---|---|---|
| **NBRl** | **NBRs** | **NDVI** | **P7** | **P6** | **P5** | **P4** | **P3** | **P2** | **P1** | |
| -3.01 | -5.37 | -1.18 | -0.01 | -0.01 | 0 | 0.02 | 0.04 | 0.07 | 0.09 | Min |
| 21.96 | 6.78 | 0.87 | 1.59 | 1.59 | 0.65 | 0.71 | 0.67 | 0.66 | 0.64 | Max |
| 9.475 | 0.705 | -0.155 | 0.79 | 0.79 | 0.325 | 0.365 | 0.355 | 0.365 | 0.365 | Mean |
| 0.23 | 0.19 | 0.23 | 0.09 | 0.09 | 0.07 | 0.07 | 0.04 | 0.03 | 0.02 | sdev |

| **Post-Fire** | | | | | | | | | | |
|---|---|---|---|---|---|---|---|---|---|---|
| **NBRl** | **NBRs** | **NDVI** | **P7** | **P6** | **P5** | **P4** | **P3** | **P2** | **P1** | |
| -0.88 | -0.92 | -0.67 | 0 | 0 | 0.01 | 0.04 | 0.05 | 0.08 | 0.1 | Min |
| 0.88 | 0.78 | 0.8 | 1.49 | 1.49 | 1.47 | 0.65 | 0.56 | 0.5 | 0.46 | Max |
| 0 | -0.07 | 0.065 | 0.745 | 0.745 | 0.74 | 0.345 | 0.305 | 0.29 | 0.28 | Mean |
| 0.14 | 0.11 | 0.12 | 0.08 | 0.09 | 0.07 | 0.06 | 0.04 | 0.03 | 0.02 | sdev |

| **Changes** | | | | | | | | | | |
|---|---|---|---|---|---|---|---|---|---|---|
| **NBRl** | **NBRs** | **NDVI** | **P7** | **P6** | **P5** | **P4** | **P3** | **P2** | **P1** | |
| -2.53 | -4.93 | -1.18 | -1.45 | -1.37 | -1.18 | -0.44 | -0.4 | -0.35 | -0.3 | Min |
| 22.46 | 7.17 | 1.22 | 1.36 | 0.83 | 0.5 | 0.51 | 0.52 | 0.53 | 0.5 | Max |
| 9.965 | 1.12 | 0.02 | -0.045 | -0.27 | -0.34 | 0.035 | 0.06 | 0.09 | 0.1 | Mean |
| 0.22 | 0.19 | 0.21 | 0.07 | 0.08 | 0.07 | 0.06 | 0.04 | 0.02 | 0.02 | sdev |

Before burning, the highest reflectance lied in the SWIR-1 and SWIR-2 channel (band 6 and band 7). Also after burning, the highest reflectance lied in the SWIR-1 and SWIR-2 channel (band 6 and band 7) (Fig.4). Based on the graph, however, generally, there can be understood that the fires will decrease reflectance on all channels, from visible, Near Infra-Red, and Short Wave Infrared bands. Table 1 shows the changes in reflectance and index values due to fires.

When compared between forest land fires in mountainous regions with lowland regions. both regions will different reflectance patterns in the visible spectrum (Kaufman, Y. J., & Remer, L. A. 1994). fires in lowland regions, the decrease in reflectance occurs only in the visible spectrum. In the Near spectrum, it will increase. While mountain region will decrease the reflectance value across the entire spectrum from the visible to the SWIR.

Fig. 5 show pre-fires and post-fires images of NDVI, NBRS, and NBRL derived from Landsat-8. Based on the measurement results it can be seen that the fires will cause a decrease in the value of NBRS, and NBRL. the value of NBRS decreased from 0.705 to -0.07 . While the value of NBRL decreased from 9.475 to 0 .

**Table 2.** Normalized Distance For Spectral Bands and Indexes of Landsat-8.

| NBRl | NBRs | NDVI | P7 | P6 | P5 | P4 | P3 | P2 | P1 |
|---|---|---|---|---|---|---|---|---|---|
| 25.608 | 2.583 | 0.628 | 0.264 | 0.25 | 2.964 | 0.153 | 0.625 | 1.25 | 2.125 |

The variables of P1, P2, P5, NBRS, and NBRL showed the D-value > 1, therefore they have good separability to discriminate burned and unburned areas Table 2. This result is able to uncover the ability of P1, P2, P5, NBRS, and NBRL in a separate area burned and unburned by the fires. One other important thing is that this result also showed that NBRL parameter has the highest of D-value compared with another parameter of a single band. Therefore, those variables were done as the threshold. The threshold based on the mean (μ) and deviation standard (σ) values Table 1. Based on the normal distribution assumption, be chosen the values of $\mu \pm 1\ \sigma$ as the threshold values for burned areas discrimination.

Burned areas pixels are extracted by applying the thresholds of post and changes of the variables. The pixel was defined as burned areas if meet the following criteria:

$$BA(NBRL)ij = \begin{cases} dNBRLij & \geq 9.745 \\ NBRLpostij & \leq 0.14 \end{cases}$$

Where:
BA(NBRL)ij is burned area pixel based on NBRL.
dNBRLij = NBRL(pre-fires)ij - NBRL(post-fires)ij.

The result of the implementation of this formula can be seen in Fig.6. When the results were compared with the appearance of the Landsat-8 RGB color composite image 654 Fig.3, then visually can be seen that the results of parameter estimation using NBRL already provides a good overview of the results.

## CONCLUSION

On the lowland regions, based on Landsat-8, the burned area shows the highest reflectance lied in the SWIR-1 and SWIR-2 channel (band 6 and band 7). The fires will decrease reflectance on all channels, from visible, and Near Infra-Red bands, whereas band 5 has the greatest increase in reflectance value. The fires also will cause a decrease in the value of NBRs, and NBRL. NBRL parameter shows the highest values of D-values (most sensitive), to detect the burned area. The results show that, compared to ρ5, NDVI, and NBRS, Normalized Burn Ratio long (NBRL) provides better results in detecting burned areas.

## REFERENCES


1. Anaya, J. A., Sione, W. F., & Rodríguez-Montellano, A. M. (2018). Identificación de áreas quemadas mediante el análisis de series de tiempo en el ámbito de computación en la nube. *Revista de Teledetección*, (51), 61-73.
2. Gao, B. C. (1995). Normalized difference water index for remote sensing of vegetation liquid water from space. In Imaging Spectrometry (Vol. 2480, pp. 225-237). International Society for Optics and Photonics.
3. González-Alonso, F., Franco, C., Vargas, F., & Armenteras, D. (2013). A new algorithm for mapping burned areas in Colombia. *Agronomía Colombiana*, *31*(2), 234-242.
4. Kaufman, Y. J., & Remer, L. A. (1994). Detection of forests using mid-IR reflectance: an application for aerosol studies. *IEEE Transactions on Geoscience and Remote Sensing*, *32*(3), 672-683.
5. Key, C. H., & Benson, N. C. (1999). The Normalized Burn Ratio (NBR): A Landsat TM radiometric measure of burn severity. *United States Geological Survey, Northern Rocky Mountain Science Center.(Bozeman, MT)*.
6. Landsat, U. S. G. S. (2015). 8 (L8) data users handbook. *LSDS-1574 Version*, *3*.
7. Liang, S., Fang, H., & Chen, M. (2001). Atmospheric correction of Landsat ETM+ land surface imagery. I. Methods. IEEE Transactions on Geoscience and Remote Sensing, 39(11), 2490-2498.
8. Long, T., Zhang, Z., He, G., Jiao, W., Tang, C., Wu, B., ... & Yin, R. (2019). 30 m Resolution Global Annual Burned Area Mapping Based on Landsat Images and Google Earth Engine. *Remote Sensing*, *11*(5), 489.
9. Nugroho, J. T., & Arifin, S. (2014, September). Performance test parameters of remote sensing for

identification burned area using Landsat-8. In *2014 International Conference on ICT For Smart Society (ICISS)* (pp. 91-100). IEEE.

10. Rouse, J. W., Haas, R. W., Schell, J. A., Deering, D. H., & Harlan, J. C. (1974). Monitoring the vernal advancement and retrogradation (Greenwave effect) of natural vegetation, NASA/GSFC, Greenbelt, MD.
11. Roy, D. P., Huang, H., Boschetti, L., Giglio, L., Yan, L., Zhang, H. H., & Li, Z. (2019). Landsat-8 and Sentinel-2 burned area mapping-A combined sensor multi-temporal change detection approach. *Remote Sensing of Environment*, *231*, 111254.
12. Suwarsono, H. L., Fitriana, H. L., Prasasti, I., & Khomarudin, M. R. (2018). Mapping burned areas from landsat-8 imageries on mountainous region using reflectance changes. In *MATEC Web of Conferences* (Vol. 229, p. 04012). EDP Sciences.
13. Todd, J., Melanie, K., Joshua, D., Gail, L., Jeff, T., Nicole, M., ... & John, L. (2017). Mapping burned areas using dense time-series of Landsat data. *Remote sensing of environment*.
14. Trisakti, B., Nugroho, U. C., & Zubaidah, A. (2017). Technique for identifying burned vegetation area using Landsat 8 data. *International Journal of Remote Sensing and Earth Sciences (IJReSES)*, *13*(2), 121-130.
15. Vedovato, L. B., Jacon, A. D., Pessôa, A. C. M., Lima, A., Oliveira, L. E., & De Aragão, C. R. U. Z. (2015). Detection of burned forests in Amazonia using the normalized burn ratio (NBR) and linear spectral mixture model from Landsat 8 images. *João Pessoa-PB, Brasil*.